ANALYSE POTENZIELLER THERMALMANAGEMENT-SYSTEME FÜR ELEKTRIFIZIERTE KURZSTRECKENFLUGZEUGE IM EXZELLENZCLUSTER SE²A

ANALYSIS OF POTENTIAL THERMAL MANAGEMENT SYSTEMS FOR ELECTRIC SHORT-RANGE AIRCRAFT IN THE CLUSTER OF EXCELLENCE SE²A

M. Nozinski*†, S. Kabelac*†

* Leibniz University Hannover, Institute of Thermodynamics, An der Universität 1, 30823 Garbsen, Germany
 † Cluster of Excellence SE²A – Sustainable and Energy-Efficient Aviation, Technische Universität Braunschweig, Universitätsplatz 2, 38106 Braunschweig, Germany

Abstract

Electric aircraft powered by fuel cells and batteries represent a promising avenue for reducing emissions from the aviation industry and meeting the ambitious climate goals. However, the increasing waste heat of the powertrain components and their low permitted operating temperatures place significant demands on the thermal management system. This study delineates the methodological approach employed in the Custer of Excellence "Sustainable and Energy-Efficient Aviation" (SE²A) to design and simulate a thermal management system for electric aircraft. The workflow is divided into four fundamental steps: a thermal analysis to identify heat sources and sinks, a generation of potential system configurations, design of the thermal components for a specific design point, and performance evaluation of the system in an off-design analysis. The thermal requirements are primarily determined by the fuel cell, which accounts for a proportion of 80 to 95 % of the total waste heat, while the liquid hydrogen fuel tank can only reduce the total amount of heat by 5 % when considered as a heat sink. The remaining waste heat must be dissipated by a heat exchanger to the environmental air. The optimization of these heat exchangers is conducted using a genetic algorithm, with the constraints imposed by the available installation space and aircraft-related boundary conditions. The optimization process yields a Pareto front comprising potential designs with varying drag and weight characteristics. Exemplary designs are investigated in detail over the course of a flight mission, revealing the potential for drag reduction during cruise with the implementation of an appropriate control strategy.

Keywords

Thermal management system; Electric aircraft; Numerical optimization

NOMENCLATURE		Subscripts		
NOMENCL A \dot{C} c_p D F G h	area heat capacity rate specific isobaric heat capacity drag objective function constraint specific enthalpy	m² W/K J/(kg K) N - - J/kg	act com cond cool irr is m	activation compressor concentration conduction cooling irreversible isentropic mechanical
I m \dot{m} NTU P \dot{Q} R_i T	current mass mass flow rate number of transfer units power rate of heat flow internal resistance temperature	A kg/s kg/s · · · · · · · · · · · · · · · · · · ·	rec rev theo turb Acronyms AC DC ECS	recirculation reversible theoretical turbine alternating current direct current environmental control system
$egin{aligned} U_v \ UA \ W \ x \end{aligned}$ Greek sym ΔT_m $arepsilon \ \eta \ artheta \ ho$	voltage overall heat transfer coefficient weight design variable bols mean temperature difference effectiveness efficiency Celsius temperature density	V W/K N - K - °C m³/kg	HDTO HEX IHEX LH2 (PEM)FC PE RHEX SE²A SHEX TMS TRL VCC	hot-day take-off heat exchanger internal heat exchanger liquid hydrogen (polymer electrolyte membrane) fuel cell power electronics ram air heat exchanger Sustainable and Energy-Efficient Aviation skin heat exchanger thermal management system technology readiness level vapor compression cycle

1. INTRODUCTION

In consideration of the increasingly apparent consequences of climate change, the European Union has established the objective of achieving climate neutrality by the year 2050 [1]. In accordance with this plan, the FLIGHTPATH 2050 outlines specific objectives for the aviation industry, which include a significant reduction in the emissions and noise pollution of future aircraft [2]. The realization of these goals is contingent upon the implementation of innovative technologies, improvements in operations and infrastructure, deployment of sustainable aviation fuels, and investments in out-of-sector carbon reduction market-based measures [3]. With regard to novel technologies, there is a considerable potential for the complete replacement of carbon-based fuels through the introduction of electric powertrains, thereby achieving zero emissions. all-electric aircraft are intended primarily for the short-range market, given that their low power and energy densities are incompatible with the power and energy requirements of long-range flights [4, 5].

These electric powertrains, comprising fuel cells, batteries, power electronics, and electric motors, are responsible for dissipating a considerable quantity of waste heat at a relatively low temperature. The heat sources are situated in different locations within the aircraft, necessitating their incorporation into a thermal management system (TMS) that not only ensures heat dissipation to the environmental air but also exhibits a high power density [6]. Furthermore, the TMS must demonstrate reliability throughout the entirety of the flight mission, a requirement that introduces additional complexity due to the variability of environmental conditions and the diverse power requirements associated with different operating points [7].

In the context of the Cluster of Excellence "Sustainable and Energy-Efficient Aviation" (SE²A), research is being conducted with the objective of identifying potential solutions for a more climate-friendly future in aviation [8,9]. The interdisciplinary network encompasses a comprehensive range of research areas, including an assessment of the air transport system (cluster area A), improvements to flight physics and vehicle systems (cluster area B), and the implementation of novel energy storage and conversion processes for aircraft (cluster area C). Within cluster area C, the challenges of the design and integration of a TMS are addressed in project C5.1, "Total Thermal Management Design and Optimization," through a holistic approach involving the development of a modular simulation framework.

The aim of this study is to present the methodological approach employed in the project to design and simulate a TMS for electric aircraft. Each step of the workflow is illustrated by means of preliminary results for an exemplary powertrain configuration, accompanied by an identification of open research questions and an outline of planned future work.

2. WORKFLOW

The general workflow employed in the project for the preliminary examination of a TMS is comprised of four principal steps.

Thermal analysis. A list of heat sources aboard an electric aircraft serves to define the thermal requirements for the TMS. The potential for different heat sinks to dissipate the waste heat is identified, and critical flight phases, as well as the design point of the TMS, are determined.

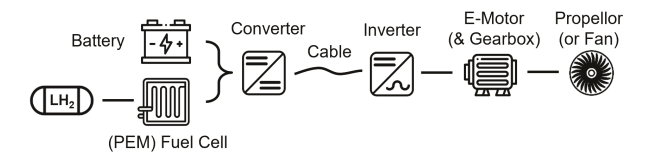


FIG 1. Electric powertrain for the study.

- System configuration. A comparative analysis of potential TMS configurations is conducted based on a list of relevant heat sources. The configurations differ in terms of interconnectivity, reliability, weight, and volume.
- 3) Component design. Models are constructed for the TMS configurations with the objective of estimating their impact on the aircraft level, namely weight, drag, and volume. A particular emphasis is placed on the heat exchanger (HEX) due to its importance for reliable heat dissipation. The components are optimized through the use of a genetic algorithm, constrained by specific aircraft-related boundary conditions.
- 4) Off-design analysis. In order to demonstrate the functionality of the TMS throughout the entirety of the flight mission, an off-design analysis is conducted. The analysis is centered upon performance data, specifically with regard to drag and power consumption at specific mission points.

It is important to note that these steps should not be viewed as a mere sequence of consecutive steps without interconnection. Rather, they should be regarded as an integrated workflow. In particular, an iteration loop between different steps is a desirable outcome. To illustrate this, the finding of a negligible weight of a heat source can result in an adjustment of the list of relevant heat sources. Similarly, the finding of an insufficient performance over the flight mission can lead to an adjustment of the design point.

The methodology employed in each step is outlined in this paper, with exemplary results provided to illustrate the process. As a baseline boundary condition, the electric powertrain depicted in Fig. 1 is utilized and sized for a similar propulsive power as for the ATR-72, with the primary power source being a polymer electrolyte membrane fuel cell (PEMFC). Given that the battery represents a unique type of thermal heat source due to its low operational temperature, it is incorporated into the powertrain. The PEMFC is sized for cruise conditions, while the battery is utilized for peak shaving during take-off and climb. The corresponding flight mission, illustrating the total propulsive power and altitude over flight time, is presented in Fig. 2 [10].

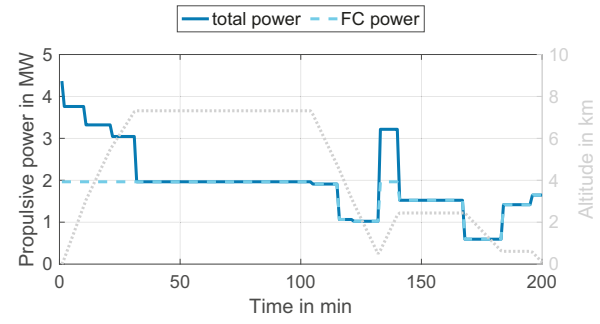


FIG 2. Flight mission for the study. The remaining peak power is provided by the battery.

The configuration of the powertrain is not directly related to the work of other groups in the cluster. Rather, it serves as an effective means of illustrating the challenges associated with TMSs. Similarly, the reference aircraft have not yet been optimized and adjusted to align with the given powertrain configuration in the cluster.

3. THERMAL ANALYSIS

In the thermal analysis, the heat sources and heat sinks are introduced in a sequential manner, with the effects of each on the flight mission subsequently demonstrated.

3.1. Heat sources

In the context of this study, a heat source is defined as a component or object that generates heat and requires cooling in order to maintain a temperature below a specified threshold. In comparison to a conventional aircraft powered by a combustion process, the electric powertrain represents a novel type of heat source in an aircraft, while other heat sources outside the powertrain have already been incorporated to some extent in modern more-electric aircraft [11].

3.1.1. Powertrain heat sources

Electric components generate heat as a consequence of thermodynamic irreversibilities. In the battery, losses arise from irreversible Joule heating \dot{Q}_{irr} and reversible entropic heating \dot{Q}_{rev} [12].

(1)
$$\dot{Q}_{battery} = \dot{Q}_{irr} + \dot{Q}_{rev} = I^2 R_i - I T \frac{\mathsf{d} U_v}{\mathsf{d} T}$$

The internal resistance R_i and the entropic coefficient $\mathrm{d}U_v/\mathrm{d}T$ are calculated from measured data as a function of the state of charge of the battery [13].

The PEMFC irreversibly generates heat due to electrochemical reactions (activation losses $U_{v,act}$), ionic and electronic conduction (ohmic losses $U_{v,ohm}$), and mass transport (concentration losses $U_{v,con}$). Based on these losses, the operating voltage U_v is calculated (see [14] for detailed information) or measured in the form of a polarization curve.

(2)
$$P_{FC} = I \left(U_{v,Nernst} - U_{v,act} - U_{v,ohm} - U_{v,con} \right)$$

The final heat loss \dot{Q}_{FC} is derived from an energy balance that incorporates all involved reactants [15].

The losses in power electronics are attributed to switching \dot{Q}_{switch} and conduction losses \dot{Q}_{cond} .

$$\dot{Q}_{PE} = \dot{Q}_{switch} + \dot{Q}_{cond}$$

A detailed calculation of both terms for converters and inverters can be found in [16] and [17], respectively,

Power losses in direct current (DC) cables are generally lower than in alternating current (AC) cables. However, losses in AC cables can be considered insignificant due to relatively short cable length between inverter and electric motor. For DC cables, the transition loss is

$$\dot{Q}_{cable,DC} = I^2 R_i$$

with resistance R_i from [18].

A comprehensive study of the loss mechanisms in electric motors is given in [19]. The largest part is caused by Joule losses [20].

$$\dot{Q}_{motor} = I^2 R_i$$

3.1.2. Heat sources outside the powertrain

Heat sources are not exclusive to the powertrain. Within the cabin, a passenger is responsible for approximately 120 W of heat generation [21]. Moreover, crew, in-flight entertainment, and payload contribute to heat generation inside the cabin and cargo hold. Combined with solar heating and aerodynamic heating at high flight speeds, the total cabin heat flow rate sums up to \dot{Q}_{cabin} with computation guidelines from [22].

Avionics for flight controls, sensors, navigation, and other electronics apart from the main powertrain also represent a heat source due to thermodynamic irreversibilities. If actuators are operated via an electric control system, their electric motor and control unit also represents a heat source. The required power is estimated from data pertaining to an A320 and scaled to the dimensions of the aircraft under consideration in this study [23]. The resulting heat losses $\dot{Q}_{actuator}$ are calculated by assuming a mechanical efficiency η_m . General and simply applicable models to calculate the power consumption of other avionics are not available in the literature. Nevertheless, to include their heat losses, the total additional power consumption outside the main powertrain is estimated as

(6)
$$P_{other} = P_{ECS}/0.75.$$

This is based on an approximation by [11] that states that the environmental control system (ECS) accounts for 75% of the total electric power consumption in conventional aircraft. The landing gear and their brakes generates heat particularly during landing through conversion of the kinetic energy of the aircraft to friction. However, as this heat generation is a highly transient process that will not be affected by the change from a combustion engine to an electric powertrain, it is not considered further in this study.

3.1.3. Heat sources in subsystems

The ECS is responsible for maintaining cabin climate and pressurization. This is typically achieved through the use of an air cycle machine. Bleed air from the engine's compressor is no longer a viable source of power for an electric aircraft, necessitating the use of an electrically driven compressor. The power consumption $P_{ECS,com}$ is estimated and scaled with the results of [22]. Similar to the electric actuators, the resulting heat loss $\dot{Q}_{ECS,com}$ is calculated with a mechanical efficiency η_m . Depending on the environmental temperature and altitude, the compressed air must be cooled prior to its expansion in a turbine.

(7)
$$\dot{Q}_{ECS,cool} = \dot{m}_{ECS,air} c_{p,air} (T_{com,out} - T_{turb,in})$$

The temperatures $T_{com,out}$ and $T_{turb,in}$ are derived from the environment and desired cabin conditions on the assumption of polytropic compression and expansion. This thermodynamic cycle absorbs the heat generated in the cabin and dissipates it to the environment. Therefore, the cabin heat flow rate \dot{Q}_{cabin} is replaced by $\dot{Q}_{ECS,com}$ and $\dot{Q}_{ECS,cool}$ as heat sources.

The battery represents a special thermal source within the powertrain, operating within a low temperature range of $20\,^{\circ}\text{C}$ and $40\,^{\circ}\text{C}$ [12]. During hot-day take-off (HDTO), cooling below environmental temperature necessitates the implementation of vapor compression cycle (VCC) [24]. The periodic compression and expansion of a refrigerant enables the heat dissipation at elevated temperatures, albeit at the cost of additional power $P_{VCC,com}$ which con-

©2024

3

sequently constitutes a heat source $\dot{Q}_{VCC,com}$. The power consumption is estimated for a polytropic compression and temperature differences of 10 K in the HEXs for the refrigerant R134 as in [24]. It should be noted that this refrigerant must be replaced in further studies due to its environmental impact and only serves here to estimate the heat flow rate. As power is added to the refrigerant, the heat flow rate to be dissipated to the environment in the condenser increases to

(8)
$$\dot{Q}_{VCC} = \dot{Q}_{battery} + P_{VCC}.$$

In order to operate the PEMFC, it is necessary to provide an air and fuel supply system. In the air system, the electrically driven compressor emerges as a heat source, as well as the required cooling of the compressed air to the operating temperature of the PEMFC. The calculation of the heat losses is analogous to that of the ECS, resulting in $\dot{Q}_{FC,cool}$ and $\dot{Q}_{FC,cool}$. If the liquid hydrogen is stored above the operating pressure of the PEMFC, no compressor is required to supply the hydrogen to the PEMFC. Only a recirculation fan is needed if hydrogen is supplied in excess, resulting in $\dot{Q}_{FC,rec}$.

3.2. Heat sinks

Heat sinks in electric aircraft are very limited because there is no hot exhaust gas to dissipate the waste heat as there is in conventional combustion aircraft. In such aircraft, the fuel tank has been used as a viable heat sink. This is also true to some extent for PEMFC-powered aircraft, as the hydrogen is stored in a liquid state at temperatures around 20 K [25]. To vaporize the hydrogen and heat it to the operating temperature of the PEMFC, internally generated heat can be used to eliminate the need for additional electric heaters. The potential of hydrogen as a heat sink is given by

(9)
$$\dot{Q}_{H2} = \dot{m}_{H2} \left(h_{H2,FC} - h_{H2,tank} \right)$$

Nevertheless, the utilization of this heat sink is constrained by the fact that the PEMFC dictates the amount of required hydrogen. Furthermore, it increases the interconnectivity between different independent subsystems, which increases the risk of failure. Ultimately, the environmental air is the only reliable heat sink that can be exploited indefinitely, but this is at the cost of large HEXs. By integrating the HEX directly into the aircraft's skin, additional anti-icing systems could be omitted [26].

3.3. Flight Mission Analysis

The application of the aforementioned equations to the flight mission in Fig. 2 yields a mission-dependent heat loss and heat sink profile. All assumptions alongside permitted temperatures of the components are given in App. A. The profile is influenced not only by the varying propulsive power during different flight phases but also by the deviating efficiencies observed during partial load.

3.3.1. Heat losses

The heat loss profile of all combined heat sources is presented in Fig. 3. Although the propulsive power declines to approximately 50 % from take-off to cruise, the heat losses exhibit a relatively minor decrease. It is only during descent that the total heat losses begin to decline significantly, and it increases once more during the aborted landing.

The proportion of each heat source to the total heat losses during take-off is illustrated in Fig. 4a. The PEMFC accounts

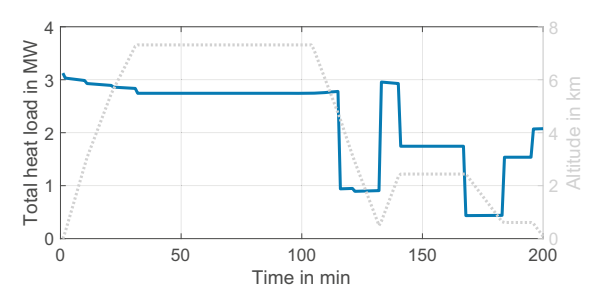
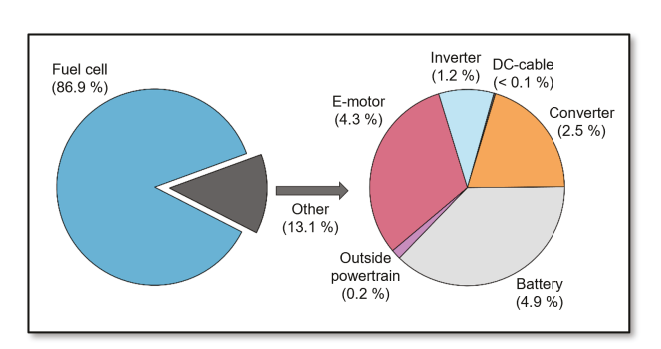


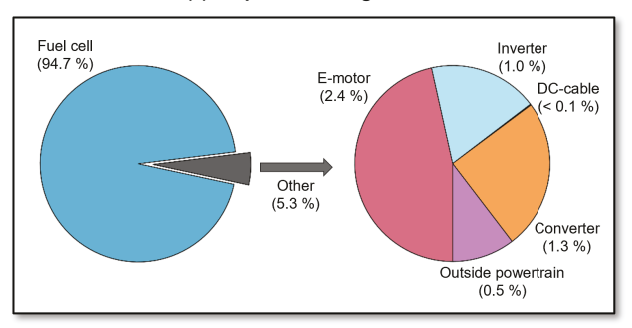
FIG 3. Heat loss profile of all combined heat sources.

for 87% of the heat losses, reflecting its relatively low efficiency. The remaining share is predominantly attributed to the electric motor, inverter, converter, and battery of the powertrain. Heat sources outside the powertrain only account for less than 1% of the total heat losses, which underscores the growing significance of the TMS for electric aircraft.

By comparing the heat distribution during take-off to the heat distribution during cruise in Fig. 4b, it is noticeable that the PEMFC's proportion of the total heat losses even increases. This is due to the fact that the PEMFC is sized for cruise operation in this study, whereby its power output and thus its heat load remains constant throughout take-off and cruise. The battery is only active for peak power shaving during cruise and climb, and consequently does not contribute to the heat losses during cruise. Given that the propulsive power declines during cruise, the heat losses of the electric motor, inverter, and converter likewise decrease. However, the significant influence of the PEMFC results in only a minor reduction in the total heat losses, as initially observed in Fig. 3. It should be noted that this behavior is altered when the battery is omitted and the PEMFC is sized for take-off. The reduced propulsive power, combined with enhanced efficiency during part-load operation, would result in an intense heat loss peak during take-off.



(a) Proportion during take-off.



(b) Proportion during cruise.

FIG 4. Proportion of heat sources in the total heat loss.

©2024

4

3.3.2. Hydrogen heat sink potential

The potential of hydrogen as a heat sink as defined in Eq. 9 is shown in Fig. 5. The qualitative profile aligns the power output of the PEMFC, as both are coupled by the hydrogen mass flow rate. During take-off and cruise, a heat flow rate of approximately 150 kW is required to vaporize and heat up the hydrogen, indicating that only 5% of the total heat losses could be embedded to the hydrogen supply.

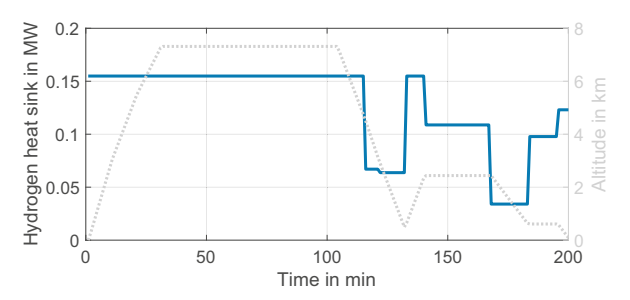


FIG 5. Required heat flow rate for processing hydrogen depicted as a potential heat sink for other heat sources.

3.3.3. Design point

The heat loss profile gives rise to the question of a design point, since no clear peak in the heat losses can be identified for the investigated powertrain configuration. However, it is not only the heat flow rate but also the temperature difference that is decisive in determining the critical operating point for the TMS. The size and thus the weight of a HEX is governed by its overall heat transfer coefficient UA, derived from

$$(10) UA = \frac{\dot{Q}}{\Delta T_m}$$

where ΔT_m is the temperature difference between component and environmental air. The behavior of UA over the flight mission relative to its value during HDTO is depicted in Fig. 6 for the main heat sources within the powertrain. The relative value for all components is below one due to a decrease in air temperature with altitude [27]. Therefore, the highest overall heat transfer coefficient and, consequently, the largest HEX is required at take-off. This confirms the take-off as the design point for the TMS and highlights the issue of oversizing the TMS for take-off in order to ensure reliable operation. Nevertheless, the correct function the TMS must be checked across all flight conditions, since the decreasing density with height may result in a diminished air flow for a fixed intake size.

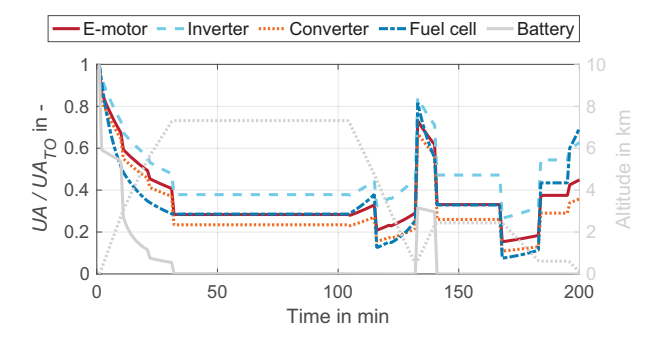


FIG 6. Overall heat transfer coefficient relative to its value during take-off to find a suitable design point.

4. SYSTEM CONFIGURATION

The initial thermal analysis revealed that the heat sources in the powertrain have the greatest impact on the total heat losses, with the PEMFC being a particularly significant contributor. The DC cable exhibits relatively low heat losses, which can be effectively managed through air cooling without significant effort. A similar conclusion can be drawn with regard to the heat sources outside the powertrain. Consequently, the electric motor, the inverter, the converter, the PEMFC, and the battery represent the components of interest for the design of the TMS.

4.1. TMS components

In order to achieve high power densities at the electric component level, air cooling is presumably not a viable option. Instead, forced liquid cooling is preferred due to its high technology readiness level (TRL). Evaporative cooling is also a feasible option, however, its lower TRL for aviation application and a more sophisticated required control strategy prevent a widespread application for the first generation of commercial electric aircraft [28].

A liquid cooling cycle comprises a heat acquisition device at the heat source, e.g. a cold plate, a pump, piping, and a HEX for dissipating the heat to a heat sink. It is important to note that the aforementioned components represent only a partial list of the elements that should be included in the final cooling cycle. In addition, other essential components, such as expansion tanks, valves, and fittings, must also be incorporated into the cooling process. However, for the sake of simplicity, these will be omitted in this study.

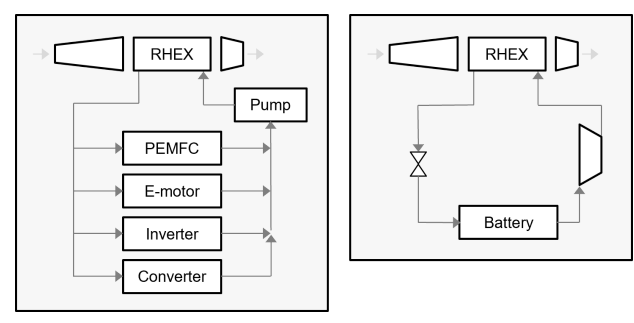
As previously stated in Sec. 3.2, the terminal heat sink is predominantly comprised of the environmental air. Consequently, a compact liquid-to-air HEX must be utilized to ensure optimal heat transfer. The most common configuration is that of a ram air heat exchanger (RHEX), which is embedded within an air duct comprising an intake, diffuser, and nozzle. The intake captures the airflow, thereby inducing drag. The airflow is then directed through the diffuser in order to reduce the pressure drop across the RHEX and finally through the nozzle to gain some recovery thrust. The installation of a puller fan is optional and serves to increase the airflow, albeit at the expense of increased power consumption [29]. As a second option, a skin heat exchanger (SHEX) is directly integrated into the surface of the aircraft, which omits drag, but requires large surface areas [30]. Moreover, a SHEX is less effective during ground operation and takeoff, when the largest HEXs are required. (cf. Fig. 6).

4.2. Exemplary TMS configurations

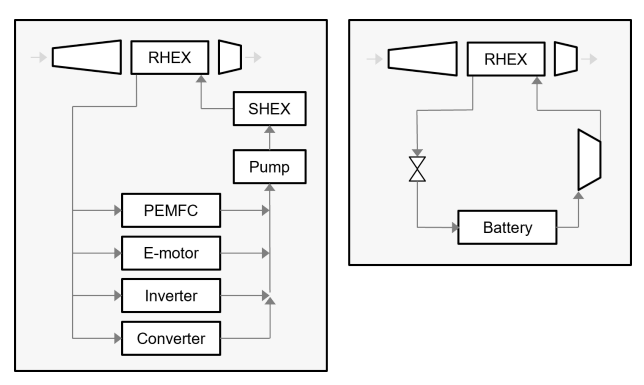
In order to demonstrate the design variety for TMSs, Fig. 7 presents potential configurations. The depicted designs do not represent the entirety of the configuration options, nor are they necessarily the optimal configurations. Rather, it is intended to illustrate the range of possible layouts, varying in complexity and interconnectivity.

The configuration depicted in Fig. 7a is relatively straightforward. All heat sources with component temperatures exceeding the environmental temperature are cooled in parallel via a single liquid cooling cycle. An even more streamlined TMS would exhibit a separate cooling cycle for each heat source. In the case of a HDTO, the battery temperature is below the environmental temperature, necessitating the use of a separate VCC.

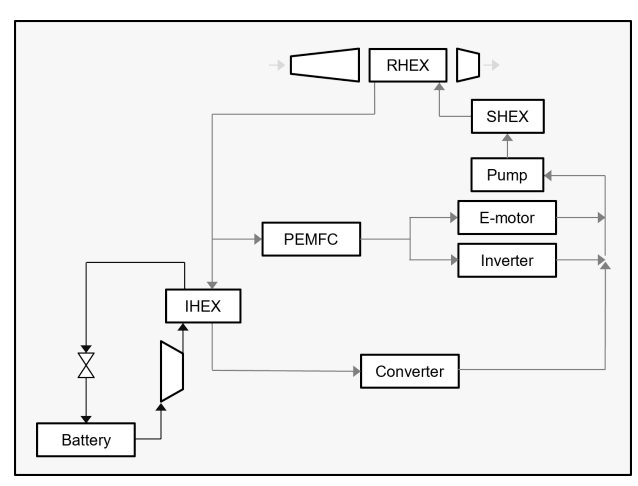
As illustrated in Fig. 7b, the second TMS extends the first configuration by incorporating a SHEX as a heat sink. Util-



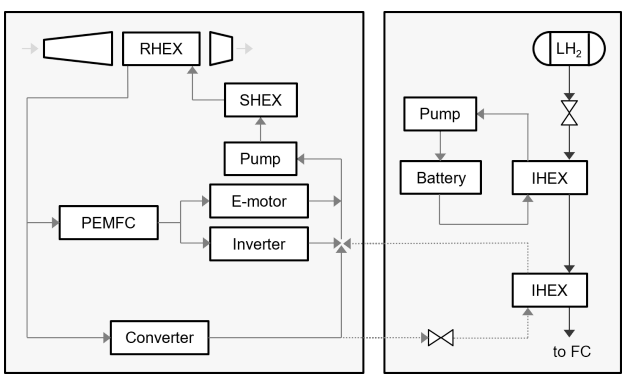
(a) TMS 1: Parallel configuration and separate battery VCC.



(b) TMS 2: Additional SHEX for heat dissipation.



(c) TMS 3: Integrated configuration.



(d) TMS 4: Hydrogen heat sink exploitation.

FIG 7. Different exemplary TMS configurations.

ising a SHEX alone would entail a considerable risk of insufficient heat dissipation, potentially leading to overheating of the components. To address this, a RHEX is essential for supporting the SHEX, particularly during take-off and climb.

An illustration of a more integrated TMS is provided in Fig. 7c. In contrast to a standalone RHEX for the battery, the VCC in this configuration is integrated into the primary cooling cycle via an internal heat exchanger (IHEX). Furthermore, opposing to a parallel configuration of heat sources, a combination of parallel and series configurations has been selected. However, as interconnectivity increases, the risk of failure likewise increases, thereby reducing the overall reliability of the TMS.

It is possible to eliminate the VCC entirely by integrating the cold liquid hydrogen into the TMS, as illustrated in Fig. 7d. The hydrogen provides temperatures below the maximum permitted temperature of the battery, thereby acting as a heat sink. In order to achieve precise heating of the hydrogen to the operating temperature of the PEMFC, integration of heat from an additional heat source is necessary to eliminate the need for an electric heater.

5. COMPONENT DESIGN

Once a TMS configuration has been selected, its components must be sized in order to fulfill their thermal requirements. In order to simplify this study, only liquid cooling cycles are considered, not the VCC for battery cooling. The design is limited to a comprehensive optimization of the compact liquid-to-air HEX, given its status as the most substantial and voluminous component within the TMS [31]. The coolant pump and associated piping are here not subjected to further analysis.

5.1. Component models

All subsequent component models are implemented in Dymola, based on the object-oriented Modelica modeling language [32]. The implementation permits the utilization of identical models for both sizing and rating through the modification of the prescribed input variables. The underlying equations are only discussed in brief. For a more detailed explanation, the reader is referred to [33].

The HEX is modeled in 0D using the ε -NTU method

(11)
$$\dot{Q} = \varepsilon \, \dot{C}_{min} \, \left(T_{cool,in} - T_{air,in} \right)$$

with

6

(12)
$$\varepsilon = f\left(NTU = \frac{UA}{\dot{C}_{min}}, \frac{\dot{C}_{min}}{\dot{C}_{max}}, \text{flow arrangement}\right)$$

Given a specified heat flow rate for sizing, the required heat transfer area can be calculated using well-studied correlations for the heat transfer and pressure drop coefficients. By selecting an appropriate type of HEX for aviation application, its volume and mass are determined. For off-design simulations, the entire geometry is prescribed, and the dissipated heat flow rate is calculated. In this study, a compact flat tube mini-channel HEX with louvered fins for the airside is selected due to its low airside pressure drop [34].

In order to calculate the induced drag and the entire volume of the system for the RHEX, it is necessary to add models for the intake, diffuser, and nozzle. The airflow is captured with a scoop intake due to its high pressure recovery capability and the relatively small installation space required, in comparison to flush intakes. It is followed by a two-dimensional diffuser sized for maximum pressure recovery. The nozzle is designed with a variable exit area, which allows for the adaptation of the airflow to off-design operating points. The mass of the ram air duct is added to the total mass of the HEX. In addition to the mass, the weight of the HEX is cal-

©2024

culated as

(13)
$$W = g m, \qquad g = 9.81 \,\text{ms}^{-2}$$

for a better comparison with the induced drag.

5.2. Optimization methodology

A compact HEX features a number of potential design variables, each of which has an impact on the drag, weight, and volume of the system. The ram air duct introduces a further set of design variables, making the complete system more complex. Consequently, an optimization methodology is required to ensure the most efficient design possible. This methodology can be formulated mathematically as

$$\begin{aligned} & \text{min} & F_i(x_k), & i = 1, \dots, I \\ & \text{(14)} & & \text{s.t.} \left\{ \begin{array}{ll} G_j(x_k) \leq 0, & j = 1, \dots, J \\ x_{k,min} \leq x_k \leq x_{k,max}, & k = 1, \dots, K. \end{array} \right. \end{aligned}$$

The primary aim is to minimize a objective function F_i which is a function of the design variables x_k . The objective of a HEX may be to minimize its drag, weight, or volume. The optimization problem is subject to inequality constraints G_j which likewise depend on the design variables x_k . These can be geometrical constraints as a maximum permitted length of the air duct, or operational constraints, e.g. a maximum reasonable pressure drop of the coolant. The design variables themselves are also constrained by lower and upper bounds.

In this study, a non-dominated sorting genetic algorithm II (NSGA-II) is employed for multi-objective optimization, thereby enabling the simultaneous optimization of two conflicting objectives [35]. The convergence of the algorithm results in the formation of a Pareto front, which represents the optimal solution space where no further improvement in one objective can be made without a corresponding deterioration in the other. The optimization process is implemented in Python using the Pymoo toolbox [36]. A flowchart illustrating the coupling between the optimization process in Python and the component model in Dymola is presented in Fig. 8.

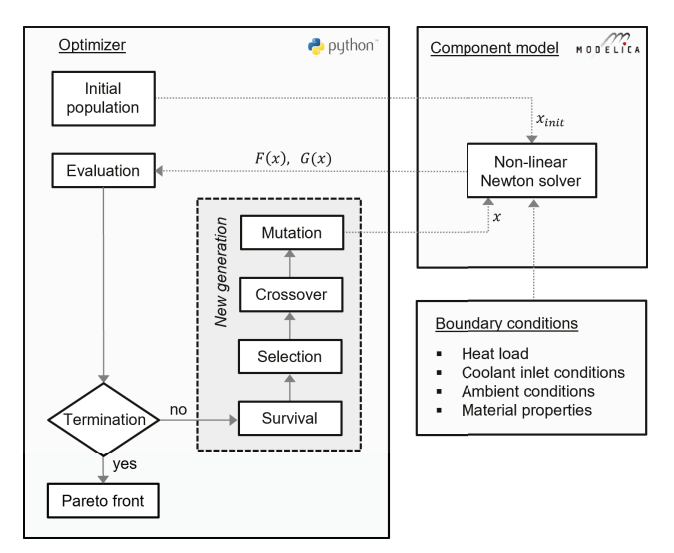


FIG 8. Flowchart of the multi-objective optimization in Python coupled with the component model in Dymola.

5.3. Sizing results

In order to demonstrate the functioning of the optimization algorithm, a test case study is conducted. The relatively simple TMS configuration depicted in Fig. 7a is selected, resulting in a total heat flow rate of approximately 3 MW, which must be dissipated to the environment by the RHEX. As a consequence of the necessity for redundancy and reliability, it is not feasible to dissipate the entire heat through a single HEX. Consequently, the total heat flow rate is divided by ten, which represents a potential distributed propulsion concept with ten nacelles, as seen in [37]. The complete list of all involved boundary conditions, design variables, and constraints is provided in App. B.

The weight and drag are chosen as objectives, resulting in the Pareto front illustrated in Fig. 9. In addition to the design heat flow rate for a single HEX of 300 kW, two further HEXs for 240 kW and 360 kW are optimized to investigate the sensitivity. Each point on the Pareto front represents a potential optimal design for a HEX that satisfies the specified boundary conditions and constraints.

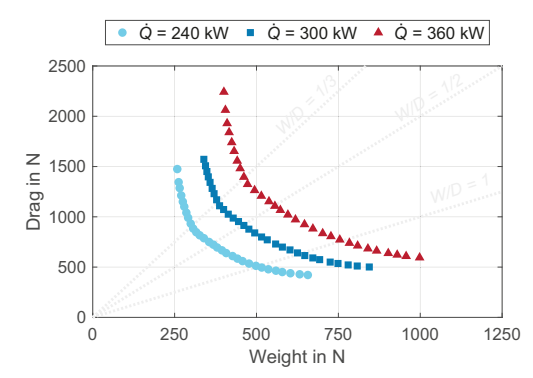
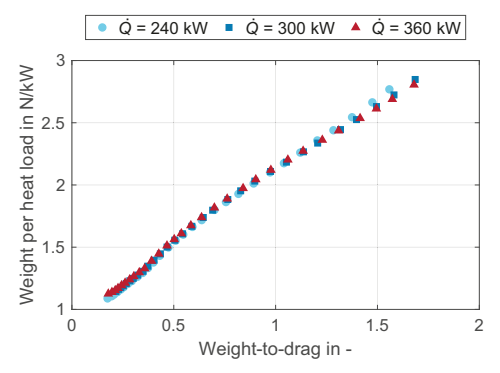


FIG 9. Pareto front for optimizing weight and drag for different design heat flow rates.

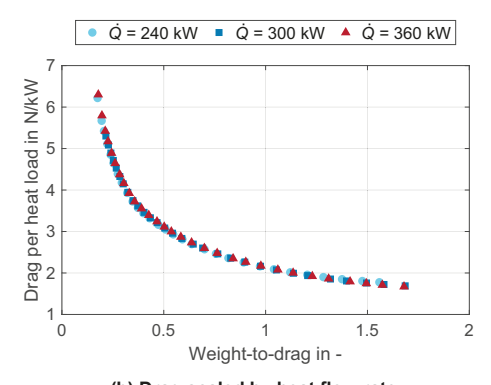
Drag and weight are two contrasting variables. Consequently, it is possible to design a lightweight HEX that induces a considerable amount of drag (on the left side of the Pareto front) or a relatively heavy HEX that induces minimal drag (on the right side of the Pareto front). It should be noted that the overall weight of the TMS will increase when additional components, such as pumps and piping, are included. However, the incorporation of these components will not directly affect the drag provided that the necessity for auxiliary air inlets is negated.

An alternative approach to visualize the results is to plot the weight-to-drag ratio W/D rather than one objective on each axis, illustrated in Fig. 10. The related counter lines of constant W/D are also shown in Fig. 9.

In Fig. 10a, the weight is plotted scaled by the respective design heat flow rate. From this perspective, it is noteworthy that the results for the different design heat flow rates are approximately equivalent. This indicates that, under the specified boundary conditions, the HEX designs can be scaled with the heat flow rate with a high degree of accuracy as a linear function of weight-to-drag ratio. A similar conclusion can be drawn with regard to the drag as illustrated in Fig. 10b, however, the dependency on the weight-to-drag ratio is not linear but hyperbolic.



(a) Weight scaled by heat flow rate.



(b) Drag scaled by heat flow rate.

FIG 10. Drag and weight with respect to the design heat flow rate as a function of weight-to-drag ratio.

6. OFF-DESIGN ANALYSIS

The HEX designed in the preceding step provides performance data for a single operating point, designated the design point. While the weight remains constant for any off-design point, the drag varies significantly over a flight mission. Therefore, it is essential to conduct a mission analysis subsequent to the design phase, particularly for specific mission phases such as climb, cruise, and descent.

6.1. Control strategy

In order to ensure the TMS's functionality under off-design conditions, a control strategy is necessary. Fig. 11 illustrates potential methods for adapting the TMS to off-design heat flow rates and environmental conditions.

Control strategy C1 manipulates the coolant's mass flow rate through the use of either a variable speed pump or a valve situated downstream of the pump. It is essential to consider the temperature difference between the flow and return temperatures $\Delta T,$ as it is directly proportional to the

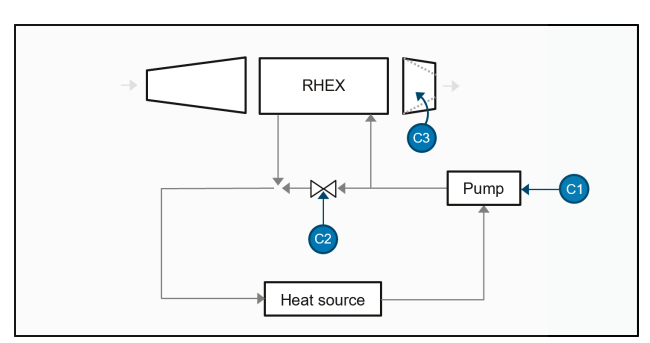


FIG 11. Potential control strategies for the TMS.

mass flow rate adjusted by the pump for a fixed heat flow rate.

$$\dot{Q} = \dot{m} c_p \Delta T$$

It is possible that high temperature differences resulting from low flow rates may give rise to thermal stresses at the heat source.

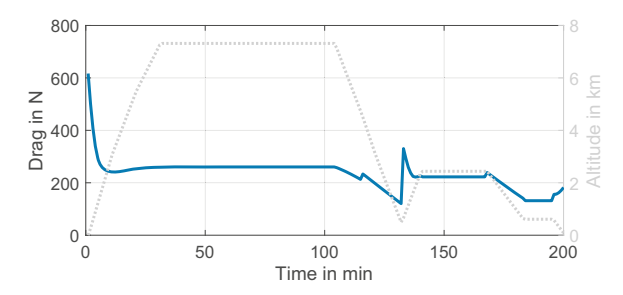
In the event that reducing the coolant flow rate is not feasible, a potential solution is the implementation of a bypass valve, as illustrated by control strategy C2. This option is straightforward to control and prevents the heat source from reaching excessively low temperatures during periods of low ambient temperature. Nevertheless, from an energetic standpoint, this approach is suboptimal since it does not result in a reduction in the power required to operate the pump.

Alternatively, it is also feasible to manipulate the airflow through the RHEX, for instance, through the use of a nozzle with an adjustable exit area. This approach is designated as control strategy C3. This option is promising in that a reduction in captured airflow will also result in a reduction in drag.

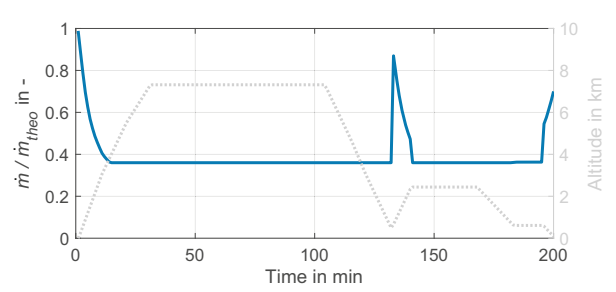
6.2. Mission analysis

The off-design calculation is demonstrated for the flight mission introduced in Fig. 2 and the corresponding heat loss profile in Fig. 3. A RHEX from the Pareto front in Fig. 9 for a designed heat flow rate of 300 kW and a weight-to-drag ratio of 1 is selected. In this exemplary study, the temperature difference is controlled by the pump, while the bypass is employed to control the temperature when necessary to maintain the coolant conditions as provided in App. B. The exit nozzle area is utilized to minimize the drag. The off-design simulation is conducted in Dymola with the identical model utilized for sizing, thereby leveraging the object-oriented programming approach.

The resulting drag is shown in Fig. 12a. It can be observed that a notable reduction in drag is achieved from take-off to cruise by decreasing the exit area, which subsequently decreases the airflow. The captured air mass flow rate is



(a) Drag over the flight mission.



(b) Relative air mass flow rate over the flight mission.

FIG 12. Performance data of the studied TMS.

demonstrated in Fig. 12b with respect to the theoretical mass flow rate

(16)
$$\dot{m}_{theo} = A_{intake} \, \rho_{air} \, V_{air}.$$

The intake spills the remaining air over the nacelle, thereby not contributing to the ram drag but causing spillage drag. It would be inadvisable to reduce the airflow rate any further, as this would result in an increased proportion of spillage drag. One potential solution would be to replace the scoop intake with a flush intake. Nevertheless, in order to demonstrate a satisfactory pressure recovery, a flush intake necessitates a significant inlet ramp length, which must be evaluated in conjunction with the available installation space [38].

7. CONCLUSION AND FUTURE WORK

In this study, the methodological approach to design and simulate a TMS for electric aircraft in the Custer of Excellence SE2A was presented. From the initial thermal analysis, it was determined that the PEMFC is responsible for over 85% of the waste heat, which can potentially reach 95 % during cruise operation. The utilization of liquid hydrogen as a heat sink has the potential to reduce the total waste heat by a mere 5 %. Given the elevated environmental temperature at ground level and the necessity for full power, the take-off was identified as the design point of the TMS. In the subsequent system configuration step, a variety of potential TMS configurations were presented, exhibiting varying degrees of complexity and interconnectivity. For the following component design, a simple liquid cooling cycle was selected. A genetic optimization methodology was presented, which generates a Pareto front with drag and weight as objectives. It was determined that within the specified heat flow rate range, both drag and weight can be scaled with satisfactory accuracy as a function of weight-to-drag ratio. In the final step, the off-design of the TMS over a flight mission was presented, along with potential control strategies. Compared to the take-off design conditions, the drag during cruise can be significantly reduced by adjusting the airflow through the use of a variable exit area nozzle.

The current and future work in this project is dedicated to improving the methodological approach, particularly in steps two, three, and four. The illustrated variety of TMS configurations will be addressed through an algorithmic approach that automatically generates and assesses potential TMS configurations using a backtracking algorithm. This eliminates the need for manual configuration generation, thus reducing the risk of inadvertently omitting a promising TMS configuration. In order to ascertain the optimal heat sink configuration for electric aircraft, the fin type selected in this study will be compared to alternative fins, together with the impact of a flush intake and the usage of a puller fan. To facilitate a rapid assessment of the TMS configurations, reduced-order models of the optimized HEXs will be developed. The off-design analysis will be augmented by a dynamic model that incorporates the thermal mass of the TMS to investigate the potential deferment of heat dissipation to subsequent flight phases.

ACKNOWLEDGMENTS

We would like to acknowledge the funding by the Deutsche Forschungsgemeinschaft (DFG, German Research Foundation) under Germany's Excellence Strategy - EXC 2163/1 - Sustainable and Energy Efficient Aviation - Project-ID 390881007.

Contact address:

nozinski@ift.uni-hannover.de

A. POWERTRAIN

Information about the selected powertrain components and their maximum permitted temperature is given in Tab. 1.

TAB 1. Powertrain components and assumptions.

component	comments & assumptions		
e-motor	$\vartheta_{max}=130^{\circ}\text{C}$, details in [20,39]		
inverter	$\vartheta_{max}=125^{\circ}\mathrm{C}$, details in [17,39]		
converter	$\vartheta_{max} = 120^{\circ}\text{C}, U_{v,grid} = 3.2\text{kV},$ details in [39,40]		
fuel cell	$\vartheta_{max}=80^{\circ}$ C, details in [41]		
battery	$\vartheta_{max} = 25^{\circ}\text{C}$, details in [12,39]		
e-motor auxiliary components	$\vartheta_{max}=120^{\circ}\mathrm{C},\eta_{m}=95\mathrm{\%}$		
compressor	$\eta_{is}=85\%$		
turbine	$\eta_{is} = 90 \%$		

B. OPTIMIZATION TEST CASE STUDY

The complete set of variables utilized in the exemplary optimization study detailed in Sec. 5.3 is presented in the following Tables 2, 3, and 4. In addition to the boundary conditions, the design heat flow rate \dot{Q} is required, which impact was shown in Fig. 9. For the design variables, the objective is to provide them in a universal format whenever feasible. For instance, non-dimensional area ratios are preferred over specific dimensions.

TAB 2. Boundary conditions for the optimization test case.

variable	unit	value
coolant return temperature	K	343.15
coolant flow temperature	K	333.15
coolant return pressure	bar	3
coolant pressure drop	bar	1
air velocity	m/s	82.31
air temperature	K	312.6
air pressure	bar	1.01325
wall thickness air duct	mm	1
wall thickness tubes	mm	0.5
wall thickness fins	mm	0.15

TAB 3. Constraint variables for the optimization test case.

variable G	unit	G _{min}	G _{max}
coolant channel height	mm	0.5	_
coolant channel width	mm	0.5	-
air duct length	m	-	2.3
air duct height	m	-	1
air duct width	m	-	1

TAB 4. Design variables for the optimization test case.

variable x	unit	X _{min}	X _{max}
air mass flow rate	kg/s	11.7	72
intake area ratio	-	2	6
diffuser area ratio	-	2	4
coolant channel aspect ratio	-	0.1	5
coolant passages per meter	1/m	20	120
louver pitch	mm	0.5	3
louver angle	0	8.4	30
louver cut length to height	-	0.63	0.95
fin pitch	mm	0.51	3.3
nozzle angle	٥	10	40

References

- [1] European Commission: Directorate General for Climate Action. Going climate-neutral by 2050: A strategic long term vision for a prosperous, modern, competitive and climate neutral EU economy. Publications Office, 2019. DOI: 10.2834/02074.
- [2] European Commission: Directorate-General for Mobility, Transport, Directorate-General for Research, and Innovation. Flightpath 2050: Europe's vision for aviation: Maintaining global leadership and serving society's needs. Publications Office, 2011. DOI: 10.2777/50266.
- [3] Air Transport Action Group. Waypoint 2050: An air transport action group project, 2021. https://aviationbe nefits.org/media/167417/w2050_v2021_27sept_full. pdf.
- [4] Ashkan Barzkar and Mona Ghassemi. Electric power systems in more and all electric aircraft: A review. *IEEE Access*, 8:169314–169332, September 2020. DOI: 10.1109/access.2020.3024168.
- [5] Andreas W. Schäfer, Steven R. H. Barrett, Khan Doyme, Lynnette M. Dray, Albert R. Gnadt, Rod Self, Aidan O'Sullivan, Athanasios P. Synodinos, and Antonio J. Torija. Technological, economic and environmental prospects of all-electric aircraft. *Nature Energy*, 4(2):160–166, December 2018. DOI: 10.1038/s41560-018-0294-x.
- [6] A.S.J. van Heerden, D.M. Judt, S. Jafari, C.P. Lawson, T. Nikolaidis, and D. Bosak. Aircraft thermal management: Practices, technology, system architectures, future challenges, and opportunities. *Progress in Aerospace Sciences*, 128:100767, January 2022. DOI: 10.1016/j.paerosci.2021.100767.
- [7] Majid Asli, Paul König, Dikshant Sharma, Evangelia Pontika, Jon Huete, Karunakar Reddy Konda, Akilan Mathiazhagan, Tianxiao Xie, Klaus Höschler, and Panagiotis Laskaridis. Thermal management challenges in hybrid-electric propulsion aircraft. *Progress in Aerospace Sciences*, 144:100967, January 2024. DOI: 10.1016/j.paerosci.2023.100967.
- [8] Valentin Batteiger, Roeland DeBreuker, Irene Dedoussi, Jan Delfs, Friedrich Dinkelacker, Ali Elham, Santiago Garcia, Jens Friedrichs, Stefan Goertz,

- Volker Grewe, Wim Haije, Christoph Herrmann, Frederic Lachaud, Axel Mertens, Joseph Morlier, Ulrike Krewer, Rolf Radespiel, Arvind Gangoli Rao, Peter Schmollgruber, Uwe Schröder, Jörg Seume, Mirjam Snellen, Andreas Strohmayer, Leo Veldhuis, Irene Villegas, Relof Vos, Henri Werij, and Feijia Yin. *Accelerating the path towards carbon-free aviation*. Exzellenzcluster Sustainable And Energy Efficient Aviation (SE²A) and Niedersächsisches Forschungszentrum Für Luftfahrt (NFL), 2023. DOI: 10.24355/DBBS.084-202207041441-0.
- [9] Sustainable and energy efficient aviation (SE²A), 2024. https://www.tu-braunschweig.de/en/se²a.
- [10] Stanislav Karpuk and Ali Elham. Influence of novel airframe technologies on the feasibility of fully-electric regional aviation. *Aerospace*, 8(6):163, June 2021. DOI: 10.3390/aerospace8060163.
- [11] Pascal Thalin. Fundamentals of electrical aircraft. SAE International, Warrendale, PA, 2018. ISBN: 978-0768093223.
- [12] Paolo Cicconi, Daniele Landi, and Michele Germani. Thermal analysis and simulation of a li-ion battery pack for a lightweight commercial EV. Applied Energy, 192:159–177, April 2017. DOI: 10.1016/j.apenergy.2017.02.008.
- [13] Daniel Ioan Stroe, Vaclav Knap, Maciej Swierczynski, and Erik Schaltz. Thermal behavior and heat generation modeling of lithium sulfur batteries. *ECS Transactions*, 77(11):467–476, July 2017. DOI: 10.1149/07711.0467ecst.
- [14] Eng. Waseem Saeed and Eng. Ghaith Warkozek. Modeling and analysis of renewable pem fuel cell system. *Energy Procedia*, 74:87–101, August 2015. DOI: 10.1016/j.egypro.2015.07.527.
- [15] Ryan O'Hayre, Suk-Won Cha, Whitney Colella, and Fritz B Prinz. Fuel Cell Fundamentals. John Wiley & Sons, Nashville, TN, 3 edition, 2016. ISBN: 978-1119113805.
- [16] Yosief Hailemariam Abraham, Huiqing Wen, Weidong Xiao, and Vinod Khadkikar. Estimating power losses in dual active bridge dc-dc converter. In 2011 2nd International Conference on Electric Power and Energy Conversion Systems (EPECS). IEEE, November 2011. DOI: 10.1109/epecs.2011.6126790.
- [17] Janine Ebersberger, Maximilian Hagedorn, Malte Lorenz, and Axel Mertens. Potentials and comparison of inverter topologies for future all-electric aircraft propulsion. *IEEE Journal of Emerging and Selected Topics in Power Electronics*, 10(5):5264–5279, October 2022. DOI: 10.1109/jestpe.2022.3164804.
- [18] Emanuele Fedele, Luigi Pio Di Noia, and Renato Rizzo. Simple loss model of battery cables for fast transient thermal simulation. *Energies*, 16(7):2963, March 2023. DOI: 10.3390/en16072963.
- [19] Peer-Ole Gronwald and Thorsten A. Kern. Traction motor cooling systems: A literature review and comparative study. *IEEE Transactions on Transportation Electrification*, 7(4):2892–2913, December 2021. DOI: 10.1109/tte.2021.3075844.

- [20] Ralf Johannes Keuter, Florian Niebuhr, Marius Nozinski, Eike Krüger, Stephan Kabelac, and Bernd Ponick. Design of a direct-liquid-cooled motor and operation strategy for the cooling system. *Energies*, 16(14):5319, July 2023. DOI: 10.3390/en16145319.
- [21] Mark Ahlers. An Introduction to Aircraft Thermal Management. SAE International, Warrendale, PA, 2020. ISBN: 978-0768095524.
- [22] Thomas Planès, Scott Delbecq, Valérie Pommier-Budinger, and Emmanuel Bénard. Modeling and design optimization of an electric environmental control system for commercial passenger aircraft. *Aerospace*, 10(3):260, March 2023. DOI: 10.3390/aerospace10030260.
- [23] Craig P. Lawson and James M. Pointon. Thermal management of electromechanical actuation on an allelectric aircraft. In 2008 26th Congress of the internation council of the aeronautical sciences (ICAS). Optimage Ltd., September 2008. ISBN: 0-9533991-9-2.
- [24] Walter Affonso, RenataT. Tavares, Felipe R. Barbosa, Ricardo Gandolfi, Ricardo J. N. dos Reis, Carlos R. I. da Silva, Timoleon Kipouros, Panagiotis Laskaridis, Hossein Balaghi Enalou, Andrei Chekin, Aleksey Kukovinets, Konstantin Gubernatorov, Yury Ravikovich, Nikolay Ivanov, Leonid Ponyaev, and Dmitry Holobtsev. System architectures for thermal management of hybrid-electric aircraft fut-print50. IOP Conference Series: Materials Science and Engineering, 1226(1):012062, February 2022. DOI: 10.1088/1757-899x/1226/1/012062.
- [25] Bhupendra Khandelwal, Adam Karakurt, Paulas R. Sekaran, Vishal Sethi, and Riti Singh. Hydrogen powered aircraft: The future of air transport. Progress in Aerospace Sciences, 60:45–59, July 2013. DOI: 10.1016/j.paerosci.2012.12.002.
- [26] Katsuaki Morita, Shigeo Kimura, and Hirotaka Sakaue. Hybrid system combining ice-phobic coating and electrothermal heating for wing ice protection. *Aerospace*, 7(8):102, July 2020. DOI: 10.3390/aerospace7080102.
- [27] Philip P Walsh and Paul Fletcher. Gas Turbine Performance. Blackwell Science, Philadelphia, PA, 2 edition, 2004.
- [28] Maria Coutinho, David Bento, Alain Souza, Rodrigo Cruz, Frederico Afonso, Fernando Lau, Afzal Suleman, Felipe R. Barbosa, Ricardo Gandolfi, Walter Affonso, Felipe I.K. Odaguil, Michelle F. Westin, Ricardo J.N. dos Reis, and Carlos R.I. da Silva. A review on the recent developments in thermal management systems for hybrid-electric aircraft. *Applied Thermal Engineering*, 227:120427, June 2023. DOI: 10.1016/j.applthermaleng.2023.120427.
- [29] Hagen Kellermann, Michael Lüdemann, Markus Pohl, and Mirko Hornung. Design and optimization of ram air-based thermal management systems for hybridelectric aircraft. *Aerospace*, 8(1):3, December 2020. DOI: 10.3390/aerospace8010003.
- [30] Hagen Kellermann, Anaïs Luisa Habermann, and Mirko Hornung. Assessment of aircraft surface heat exchanger potential. *Aerospace*, 7(1):1, December 2019. DOI: 10.3390/aerospace7010001.

- [31] Jeffryes W. Chapman, Hashmatullah Hasseeb, and Sydney L. Schnulo. Thermal management system design for electrified aircraft propulsion concepts. In AIAA Propulsion and Energy 2020 Forum. American Institute of Aeronautics and Astronautics, August 2020. DOI: 10.2514/6.2020-3571.
- [32] Mike Dempsey. Dymola for multi-engineering modelling and simulation. In 2006 IEEE Vehicle Power and Propulsion Conference, page 1–6. IEEE, September 2006. DOI: 10.1109/vppc.2006.364294.
- [33] Marius Nozinski, Behnam Parizad Benam, Carlo De Servi, Stephan Kabelac, and Chiara Falsetti. Physically based heat exchanger sizing method for the thermal management system of all-electric regional aircraft. *Journal of Physics: Conference Series*, 2766(1):012101, May 2024. DOI: 10.1088/1742-6596/2766/1/012101.
- [34] Ramesh K Shah and Dusan P Sekulic. Fundamentals of heat exchanger design. John Wiley & Sons, Nashville, TN, July 2003.
- [35] K. Deb, A. Pratap, S. Agarwal, and T. Meyarivan. A fast and elitist multiobjective genetic algorithm: NSGA-II. *IEEE Transactions on Evolutionary Computation*, 6(2):182–197, April 2002. DOI: 10.1109/4235.996017.
- [36] Julian Blank and Kalyanmoy Deb. Py-moo: Multi-objective optimization in Python. IEEE Access, 8:89497–89509, April 2020. DOI: 10.1109/access.2020.2990567.
- [37] Chetan K. Sain, Jeffrey Hänsel, and Stefan Kazula. Conceptual design of air and thermal management in a nacelle-integrated fuel cell system for an electric regional aircraft. In AIAA AVIATION 2023 Forum. American Institute of Aeronautics and Astronautics, June 2023. DOI: 10.2514/6.2023-3875.
- [38] Drag and pressure recovery characteristics of auxiliary air inlets at subsonic speeds. 86002. ESDU International PLC, London, England, June 2004. ISBN: 978-0856795541.
- [39] Janine Ebersberger, Leon Fauth, Ralf Keuter, Yongtao Cao, Yannik Freund, Richard Hanke-Rauschenbach, Bernd Ponick, Axel Mertens, and Jens Friebe. Power distribution and propulsion system for an allelectric short-range commuter aircraft—a case study. *IEEE Access*, 10:114514–114539, October 2022. DOI: 10.1109/access.2022.3217650.
- [40] Janine Ebersberger, Ralf Johannes Keuter, Bernd Ponick, and Axel Mertens. Power distribution and propulsion system for an all-electric regional aircraft. In 2023 IEEE International Conference on Electrical Systems for Aircraft, Railway, Ship Propulsion and Road Vehicles & International Transportation Electrification Conference (ESARS-ITEC), volume 8, page 1–7. IEEE, March 2023. DOI: 10.1109/esarsitec57127.2023.10114868.
- [41] Martin Staggat, Jonas Ludowicy, Victor Bahrs, Antje Link, and Stefan Kazula. Modelling of a battery supported fuel cell electric power train topology for a regional aircraft. *Journal of Physics: Conference Se*ries, 2526(1):012061, June 2023. DOI: 10.1088/1742-6596/2526/1/012061.